Article

Quantum-Chemical Modeling of the Catalytic Activity of Graphene Doped with Metal Phthalocyanines in ORR

Kirill Y. Vinogradov [1], Anzhela V. Bulanova [1,*], Roman V. Shafigulin [1], Elena O. Tokranova [1] and Hong Zhu [2]

1   Department of Physical Chemistry and Chromatography, Samara University, 443086 Samara, Russia;
    winyur@yandex.ru (K.Y.V.); shafiro@mail.ru (R.V.S.); fileona@mail.ru (E.O.T.)
2   State Key Laboratory of Chemical Resource Engineering, Department of Organic Chemistry,
    Institute of Modern Catalysis, College of Chemistry, Beijing University of Chemical Technology,
    Beijing 100029, China; zhuho128@126.com
*   Correspondence: av.bul@yandex.ru

Abstract: The active centers of carbon catalysts doped with cobalt, nickel, copper, manganese, zinc, and chromium were modeled by density functional theory methods. Likewise, the thermodynamics of the oxygen reduction reaction (ORR) on model catalysts were determined. The features of the chemical properties of chromium-containing material, namely its spontaneous oxidation into the hydroxo form, were revealed. In addition, it was established that among the studied catalysts, graphene doped with cobalt showed the best properties.

Keywords: electrochemical oxygen reduction; ORR; graphene; doping; transition metals; quantum chemical method; DFT

1. Introduction

In today's world, mankind is faced with a dilemma: the need for electricity is increasing rapidly and the world's main present natural energy sources are non-renewable. The efficiency of solar panels and wind turbines is extremely dependent on weather and climatic conditions. Now more than ever, the search for alternative sources of electricity is urgent. Fuel cells seem to be the ideal solution to the energy shortage and tense environmental situation: fuel cells are quiet, highly efficient, and environmentally friendly. However, fuel cells have a disadvantage that has prevented them from becoming widespread—the use of expensive platinum as a catalyst. Finding an alternative to the platinum catalyst will significantly reduce the cost of fuel cells, allowing them to be used more widely.

At the moment, the search for non-platinum catalysts is an urgent aim, and carbon catalysts have shown the greatest promise [1–5]. Theoretical methods, such as quantum chemical modeling using density functional theory (DFT), are used to speed up the process of finding the optimal material [6–8]. This approach makes it possible to determine the adsorption properties of the catalyst, as well as the effect of the composition and structure of the material on the kinetics of the catalytic process, and to compare different catalytic materials without resorting to experimental analysis [9–11].

Examples of materials described both theoretically and practically are metal-free catalysts based on carbon materials doped with nitrogen, sulfur, and other non-metals. The structure of the carbon framework can be different: carbon nanofibers [12], graphene [13], carbon dots [14], or a nanoporous carbon framework [15] obtained using ionic liquid as a precursor. Metal-containing catalysts with a complex active center structure [16] or multi-component oxide catalysts [17] are also possible. Such a wide range of possible catalysts allows the material properties to be varied while searching for the most effective catalyst.

In this paper, using quantum-chemical modeling, the properties of carbon materials doped with nitrogen and cobalt, nickel, copper, chromium, manganese, and zinc in ORR, taking into account the solvent and pH of the solution, are investigated.

2. Results and Discussions

Calculations of the optimized structures of intermediates in the ORR (Figure 1) show that oxygen and intermediates during adsorption are localized on the metal atom embedded in the graphene structure.
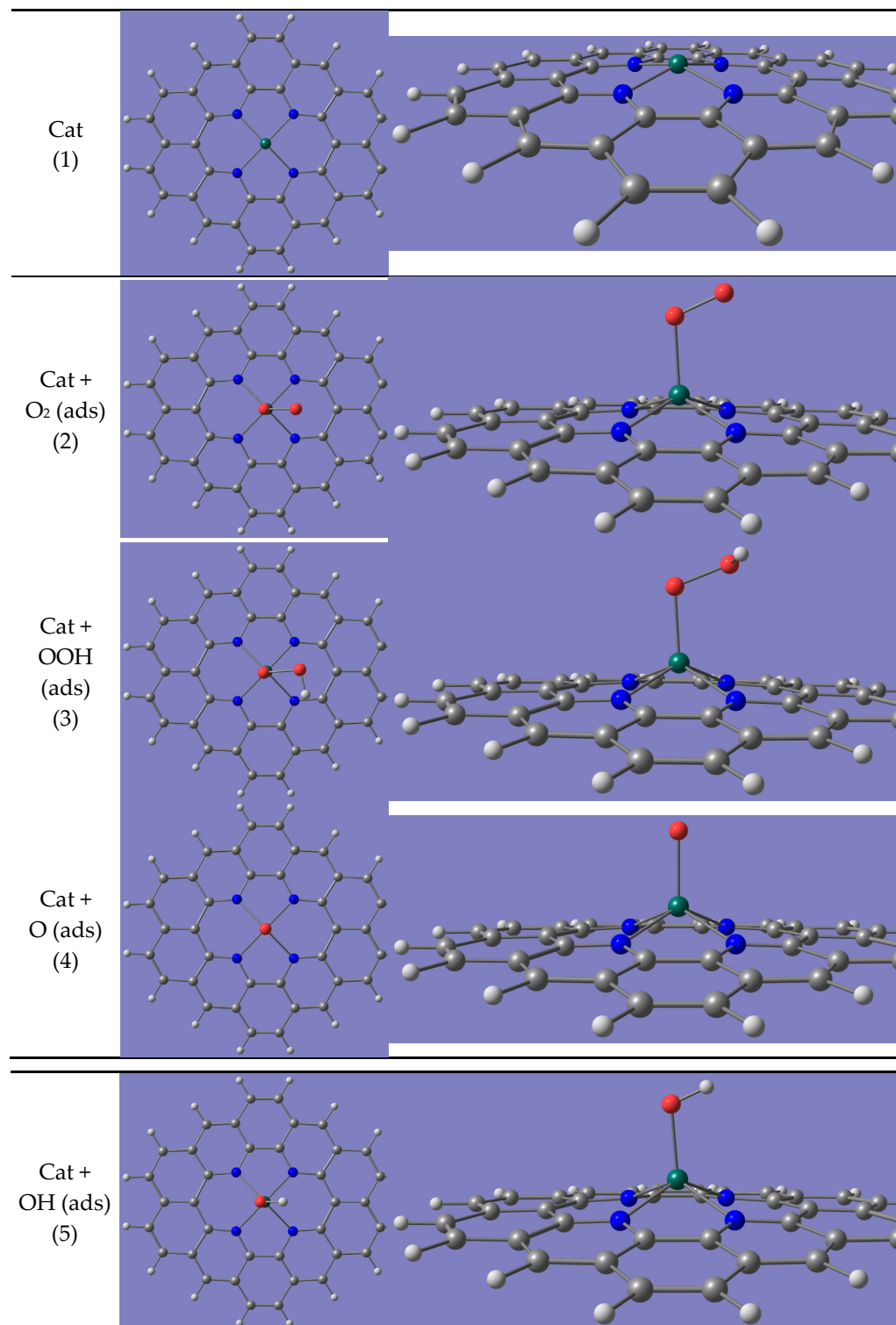
**Figure 1.** Model reaction of oxygen reduction on a catalyst containing zinc.

As a result of the simulation, the ORR energy profiles were obtained for the studied carbon materials, which are presented later in this article.

The energy profile of ORR on CrN_4 (Figure 2) is characterized by the presence of a minimum, which corresponds to the adsorbed hydroxo radical. It can be concluded that such material will spontaneously oxidize to the form $Cr(OH)N_4$, which is confirmed by the presence of such properties as those in chromium phthalocyanine [18].
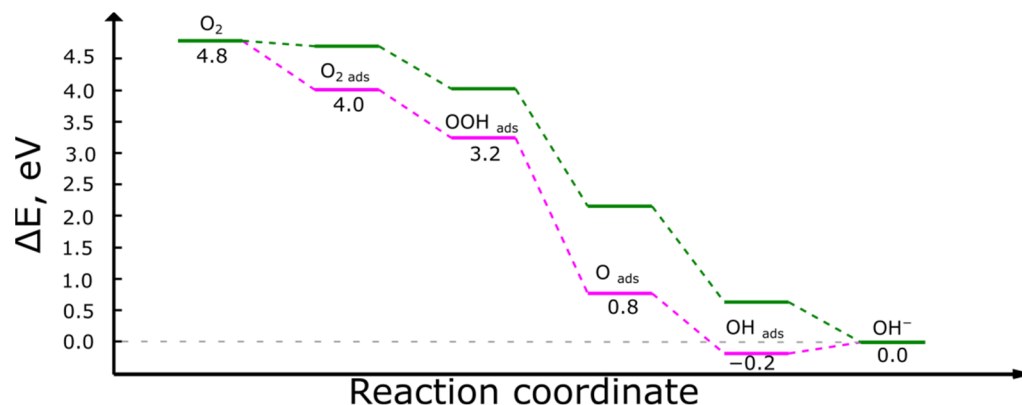
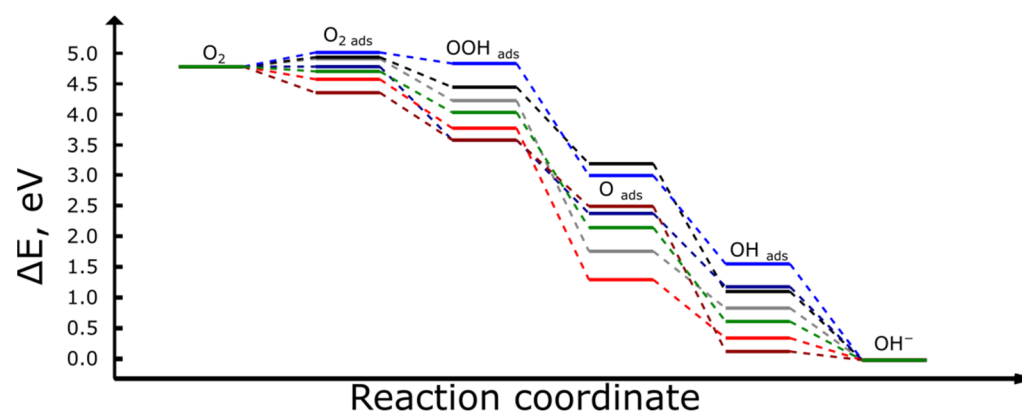**Figure 2.** Free energy profile of ORR in free form on CrN_4 (fuchsia) and $Cr(OH)N_4$ (dark green).

Thus, the $Cr(OH)N_4$ hydroxo form was chosen as the active center of the chromium-containing catalyst, which exhibits catalytic properties. An example of a complex of a catalyst and an intermediate is shown in Figure 3.
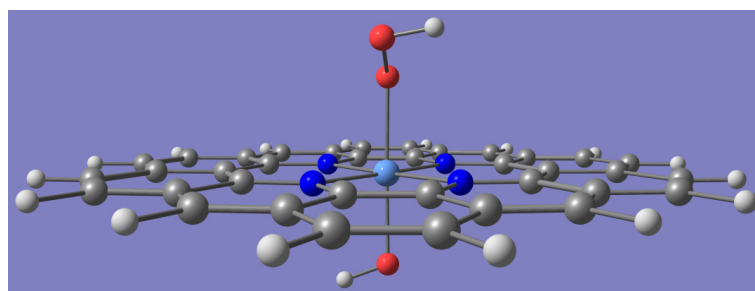
Figure 3. The structure of $Cr(OH)N_4 + OOH_{(ads)}$.

The energy profiles on all studied catalysts gradually decrease, which indicates that the choice of the ORR mechanism was made correctly (Figure 4).

Figure 4. Free energy profile of ORR on the studied catalysts: CoN_4—grey; CuN_4—black; NiN_4—blue; MnN_4—red; ZnN_4—dark red; $Cr(OH)N_4$—green. The ideal catalyst—dark blue.

According to the calculations presented in Table 1, ZnN_4 exhibits the highest affinity for oxygen. Moreover, for the CoN_4, CuN_4, and NiN_4 catalysts, an increase in the energy of

the system is observed. This suggests that, on these catalysts, energy is spent for adsorption rather than being released, which agrees with the results in [19].

Table 1. Energies of molecular oxygen adsorption.

Catalyst	CuN_4	NiN_4	MnN_4	CoN_4	ZnN_4	$Cr(OH)N_4$
G_{ads}, eV	0.15	0.23	−0.21	0.12	−0.43	−0.08
d_{Me-O}, Å	2.17	1.94	1.87	2.07	1.99	2.01
d_{O-O}, Å	1.31	1.32	1.32	1.33	1.34	1.32

The greatest elongation of the O–O bond during the adsorption of an oxygen molecule occurred on CoN_4 and ZnN_4.

Considering adsorption at individual stages (Table 2), it is easy to see that OOH adsorption is characterized by relatively low energy; oxygen atom and hydroxo radical show the highest affinity to the catalyst. The low adsorption energy of the peroxide radical can lead to an increase in the probability of the process proceeding via the undesirable 2-electron mechanism.

Table 2. Relative energies of adsorption intermediates.

Catalyst	CuN_4	NiN_4	MnN_4	CoN_4	ZnN_4	$Cr(OH)N_4$
$G_{ads\ OOH}$, eV	−0.37	0.01	−1.04	−0.60	−1.24	−0.79
$G_{ads\ O}$, eV	−1.52	−1.89	−3.58	−3.12	−2.39	−2.74
$G_{ads\ OH}$, eV	−1.53	−1.09	−2.30	−1.81	−2.52	−2.02

Strong adsorption of intermediates can also adversely affect ORR. The energies of each of the stages and overpotential are shown in Table 3.

Table 3. Free energy release on the elementary reaction stages of ORR (eV).

Catalyst	CuN_4	NiN_4	MnN_4	CoN_4	ZnN_4	$Cr(OH)N_4$
$O_2 \rightarrow OOH$	0.48	0.18	0.80	0.68	0.77	0.67
$OOH \rightarrow O$	1.08	1.83	2.47	2.45	1.08	1.88
$O \rightarrow OH$	2.26	1.44	0.96	0.93	2.37	1.52
$OH \rightarrow OH^-$	1.12	1.57	0.36	0.85	0.14	0.63
Overpotential, V	0.72	1.02	0.84	0.52	1.06	0.56

The efficiency of the process is determined by the stage with the least energy release, determining the overpotential on the catalyst, which is calculated by Formula (5). The lower the overpotential, the closer the catalyst properties are to ideal. The catalysts containing cobalt and chrome are characterized by the lowest overpotential (Figure 5). ZnN_4 and MnN_4, which showed the highest affinity for adsorbates, turned out to be inefficient due to the low energy release at the final ORR stage.

The energy profile of the ORR, taking into account the external voltage (U = 1.20 V), changes strongly with a change in the metal in the catalyst structure (Figure 6). Catalysts that include cobalt and chrome are closest to the ideal "zero-point" line.

Separately, it is worth mentioning that cobalt-containing materials are often the subject of practical research [20,21]. On the basis of calculations [22], cobalt is one of the most effective catalysts, second only to iridium and rhodium, which are less promising for commercial use due to their high price.
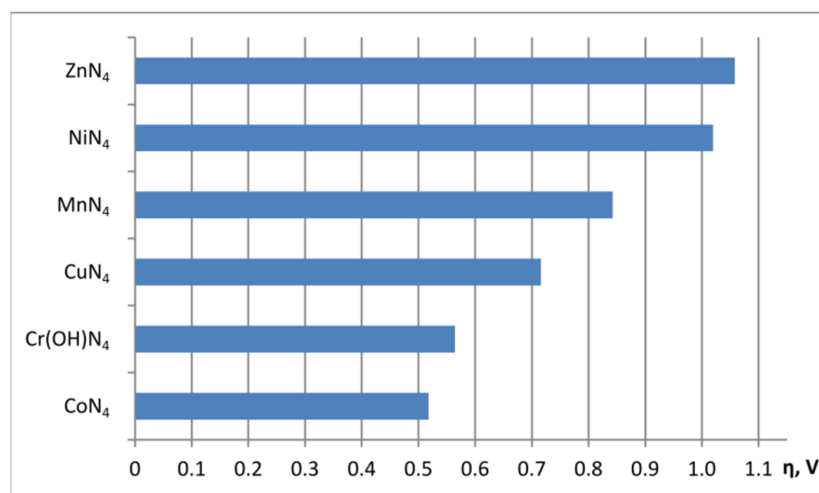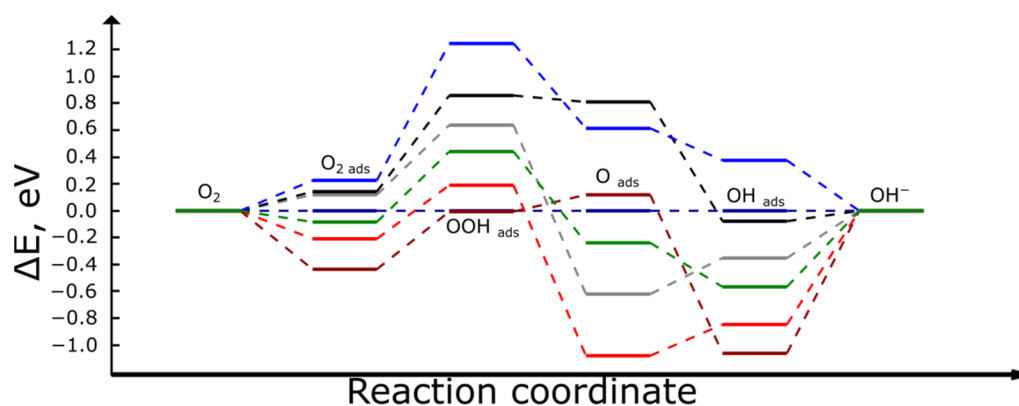
Figure 5. Overpotential on catalysts.

Figure 6. Free energy profile of ORR on the studied catalysts with a voltage of 1.20 V. CoN—grey; CuN_4—black; NiN_4—blue; MnN_4—red; ZnN_4—dark red; $Cr(OH)N_4$—green. The ideal catalyst—dark blue.

## 3. Model and Calculation Methods

Model structures were optimized and energies were calculated using the Gaussian 09 program [23]. The initial model structures and input files were created with the GaussView 6 program, and visualization was performed with the ChemCraft 1.8 program. Modeling was performed using the density functional theory (DFT) method, the B3LYP functional [24,25], and the 6–31G* basis set, which is consistent with previous studies [26]. The influence of the solvent (water) was taken into account in the self-consistent reaction field (SCRF) model [19,27].

The model structure can be described as a metal atom surrounded by four nitrogen atoms (MeN4; Me-Co, Cu, Ni, Cr, Mn, Zn) embedded in the graphene structure represented by 10 aromatic rings (Figure 7). Such porphyrin-like structures can be obtained in practice by using the phthalocyanines of the corresponding metals as the precursor [20].
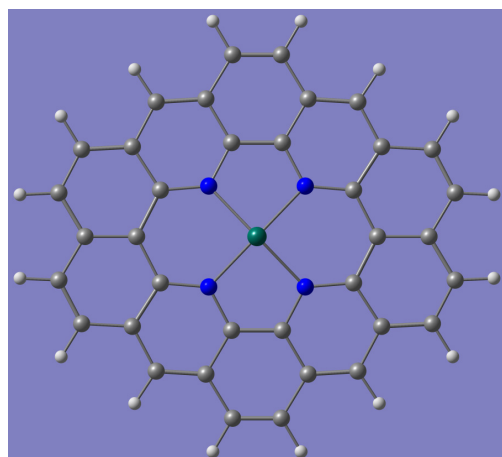
Figure 7. The structure of a model catalyst: graphene doped with four nitrogen atoms and a transition metal. Gray spheres—carbon; blue—nitrogen; white—hydrogen; green—the studied metal (Co, Cu, Ni, Cr, Mn, or Zn).

ORR in an alkaline medium follows two paths (Figure 8)—with the participation of two electrons (path 1) or four electrons (paths 2 and 3)—according to the associative (path 2) and dissociative (path 3) mechanisms [28]. A four-electron associative mechanism was chosen as a model reaction, since it prevails for this type of active centers [21].
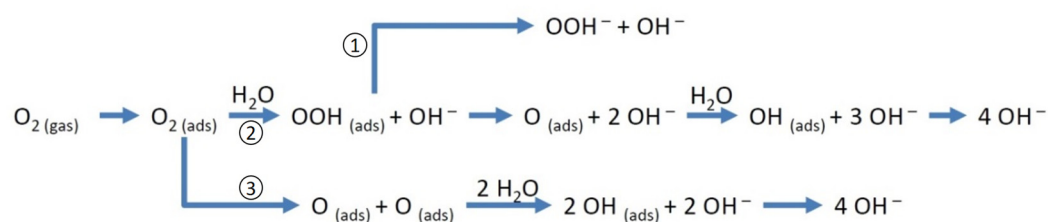
Figure 8. ORR scheme in alkaline solution (based on the scheme proposed in [28]).

The following intermediates were chosen as key points for modeling [29]:

1. $O_2 + 2\,H_2O$
2. $O_{2(ads)} + 2\,H_2O$
3. $OOH_{(ads)} + H_2O + OH^-$
4. $O_{(ads)} + H_2O + 2\,OH^-$
5. $OH_{(ads)} + 3\,OH^-$
6. $4\,OH^-$

For calculations of energies and the construction of energy dependences, the system energy was taken as being equal to the Gibbs energy calculated as the electron energy corrected for the thermal free energy [23], as shown in the following equation:

$$G = E_{ele} + E_{ZPE} + E_{tot} + k_B T - TS_{tot}, \tag{1}$$

where E_{ele} is the total electronic and nuclear repulsion energy at 0 K, E_{ZPE} is the zero-point vibrational energy, E_{tot} is the total thermal internal energy, k_B is Boltzmann's constant, S_{tot} is the system entropy, and T is the temperature (T = 298.15 K).

$$E_{tot} = E_t + E_r + E_v + E_e, \tag{2}$$

where E_t is the thermal internal energy due to translation, E_r is the internal energy due to rotational motion, E_v is the internal energy due to vibrational motion, and E_e is the internal energy due to electronic motion. The sum of the energies of the final optimized substances and the catalyst was taken as a zero level.

The adsorption energy was calculated using the following formula [30]:

$$G_{ads} = G_{system} - G_{adsorbate} - G_{catalyst}, \tag{3}$$

To determine the energy effects of the ongoing processes, the following elementary reactions occurring on the catalyst surface were identified [31]:

1.　$O_{2(ads)} + H_2O + e^- \rightarrow OOH_{(ads)} + OH^-$
2.　$OOH_{(ads)} + e^- \rightarrow O_{(ads)} + OH^-$
3.　$O_{(ads)} + H_2O + e^- \rightarrow OH_{(ads)} + OH^-$
4.　$OH_{(ads)} + e^- \rightarrow OH^-$

The above reactions correspond to the transitions of intermediates 2→3, 3→4, 4→5, and 5→6, respectively (see Table 1).

The free energy of elementary reactions (used to construct all graphs and tables) was calculated as follows taking into account the pH of the solution and the change in the electrode potential [32]:

$$\Delta G_i = \Delta G_s - eU + k_B T \cdot \ln 10 \cdot pH, \tag{4}$$

where ΔG_s is the free energy change of the system, eU is the contribution of free energy due to a change in the values of the electrode potential U, and $k_B T \cdot \ln 10 \cdot pH$ is the contribution of free energy, taking into account the pH of the solution.

According to the calculation results, the total change in the free energy in the model reaction is 4.79 eV, which is close to the ideal total change in the Gibbs free energy ORR (4.92 eV) [32].

The overpotential (η_{ORR}) was calculated as follows [22]:

$$\eta_{ORR} = 1.20 - \min\{\Delta G_1, \Delta G_2, \Delta G_3, \Delta G_4\}, \tag{5}$$

where 1.20 is one-quarter of the total free energy change and ΔG_i is the free energy change for each stage.

4. Conclusions

Based on the work done, it can be concluded that carbon materials doped with nitrogen and metals can exhibit high catalytic activity, and the ability to vary the doping metal makes it possible to select the optimal catalyst composition. Quantum-chemical calculations have shown that the best indicators have cobalt and chromium-based catalysts, and chromium is in the oxidized OH-form.

The obtained data are consistent with the results of other theoretical and experimental studies, in particular, the low overpotential for cobalt-containing materials (~0.5 V).

Author Contributions: Conceptualization: A.V.B. and R.V.S.; methodology: K.Y.V.; software: K.Y.V.; validation: A.V.B., R.V.S. and H.Z.; formal analysis: H.Z.; investigation: K.Y.V.; resources: A.V.B.; data curation: R.V.S.; writing—original draft preparation: K.Y.V.; writing—review and editing: A.V.B. and E.O.T.; visualization: K.Y.V.; supervision: A.V.B.; project administration: A.V.B.; funding acquisition: A.V.B. All authors have read and agreed to the published version of the manuscript.

Data Availability Statement: Data obtained during this study are included in the main text.

Conflicts of Interest: The authors declare no conflict of interest.

References

1. Quílez-Bermejo, J.; Morallón, E.; Cazorla-Amorós, D. Metal-free heteroatom-doped carbon-based catalysts for ORR: A critical assessment about the role of heteroatoms. *Carbon* **2020**, *165*, 434–454. [CrossRef]
2. Ratso, S.; Kruusenberg, I.; Vikkisk, M.; Joost, U.; Shulga, E.; Kink, I.; Tammeveski, K. Highly active nitrogen-doped few-layer graphene/carbon nanotube composite electrocatalyst for oxygen reduction reaction in alkaline media. *Carbon* **2014**, *73*, 361–370. [CrossRef]
3. Bouleau, L.; Pérez-Rodríguez, S.; Quílez-Bermejo, J.; Izquierdo, M.T.; Xu, F.; Fierro, V.; Celzard, A. Best practices for ORR performance evaluation of metal-free porous carbon electrocatalysts. *Carbon* **2022**, *189*, 349–361. [CrossRef]
4. Liu, Z.; Ye, D.; Zhu, X.; Wang, S.; Zou, Y.; Lan, L.; Liao, Q. ZIF-67-derived Co nanoparticles embedded in N-doped porous carbon composite interconnected by MWCNTs as highly efficient ORR electrocatalysts for a flexible direct formate fuel cell. *Chem. Eng. J.* **2022**, *432*, 134192. [CrossRef]
5. Wang, S.; Liu, Y.; Liu, X.; Chen, Y.; Zhao, Y.; Gao, S. Fabricating N, S Co-Doped Hierarchical Macro-Meso-Micro Carbon Materials as pH-Universal ORR Electrocatalysts. *Chem. Sel.* **2022**, *7*, e202200044. [CrossRef]
6. Ge, F.; Qiao, Q.; Chen, X.; Wu, Y. Probing the catalytic activity of M-N4—xOx embedded graphene for the oxygen reduction reaction by density functional theory. *Front. Chem. Sci. Eng.* **2021**, *15*, 1206–1216. [CrossRef]
7. Kuzmin, A.; Shainyan, B. Exploring of catalytic oxygen reduction reaction activity of lattice carbons of vanadium and niobium doped nitrogen codoped carbon nanotubes by density functional theory. *Authorea Prepr.* **2022**. [CrossRef]
8. Li, X.; Wang, Z.; Su, Z.; Zhao, Z.; Cai, Q.; Zhao, J. Phthalocyanine-supported single-atom catalysts as a promising bifunctional electrocatalyst for ORR/OER: A computational study. *Chem. Phys. Mater.* **2022**, *15*, 237–245. [CrossRef]
9. Yan, P.; Shu, S.; Zou, L.; Liu, Y.; Li, J.; Wei, F. Density functional theory study of active sites on nitrogen-doped graphene for oxygen reduction reaction. *R. Soc. Open Sci.* **2021**, *8*, 210272. [CrossRef]
10. Zhang, S.; Qin, Y.; Ding, S.; Su, Y. A DFT study on the activity origin of Fe-N-C sites for oxygen reduction reaction. *Chem. Phys. Chem.* **2022**. [CrossRef]
11. Lu, R.; Quan, C.; Zhang, C.; He, Q.; Liao, X.; Wang, Z.; Zhao, Y. Establishing a theoretical insight for penta-coordinated iron-nitrogen-carbon catalysts toward oxygen reaction. *Nano Res.* **2022**, *15*, 6067–6075. [CrossRef]
12. Li, H.; Ha, T.A.; Jiang, S.; Pozo-Gonzalo, C.; Wang, X.; Fang, J.; Wang, X.N. F and S doped carbon nanofibers generated from electrospun polymerized ionic liquids for metal-free bifunctional oxygen electrocatalysis. *Electrochim. Acta* **2021**, *377*, 138089. [CrossRef]
13. She, Y.; Chen, J.; Zhang, C.; Lu, Z.; Ni, M.; Sit, P.H.L.; Leung, M.K. Nitrogen-doped graphene derived from ionic liquid as metal-free catalyst for oxygen reduction reaction and its mechanisms. *Appl. Energy* **2018**, *225*, 513–521. [CrossRef]
14. Pham-Truong, T.N.; Ranjan, C.; Randriamahazaka, H.; Ghilane, J. Nitrogen doped carbon dots embedded in poly (ionic liquid) as high efficient metal-free electrocatalyst for oxygen reduction reaction. *Catal. Today* **2019**, *335*, 381–387. [CrossRef]
15. Jiao, R.; Zhang, W.; Sun, H.; Zhu, Z.; Yang, Z.; Liang, W.; Li, A. N-and S-doped nanoporous carbon framework derived from conjugated microporous polymers incorporation with ionic liquids for efficient oxygen reduction reaction. *Mater. Today Energy* **2020**, *16*, 100382. [CrossRef]
16. Martinaiou, I.; Wolker, T.; Shahraei, A.; Zhang, G.R.; Janßen, A.; Wagner, S.; Kramm, U.I. Improved electrochemical performance of Fe-NC catalysts through ionic liquid modification in alkaline media. *J. Power Sources* **2018**, *375*, 222–232. [CrossRef]
17. Hu, S.; Wang, J.; Zhang, J.; Lim, J.; Gao, Y.; Zhang, S. Engineering the electronic structure of perovskite oxide surface with ionic liquid for enhanced oxygen reduction reaction. *Appl. Catal. B Environ.* **2021**, *282*, 119593. [CrossRef]
18. Meloni, E.G.; Ocone, L.R.; Block, B.P. Phathalocyaninato (2–) chromium (III) phosphinates. *Inorg. Chem.* **1967**, *6*, 424–425. [CrossRef]
19. Marenich, A.V.; Cramer, C.J.; Truhlar, D.G. Universal Solvation Model Based on Solute Electron Density and on a Continuum Model of the Solvent Defined by the Bulk Dielectric Constant and Atomic Surface Tensions. *J. Phys. Chem. B* **2009**, *113*, 6378–6396. [CrossRef]
20. Dursun, S.; Akay, R.G.; Yazici, M.S. CVD graphene supported cobalt (II) phthalocyanine as cathode electrocatalyst for PEM fuel cells. *Int. J. Hydrogen Energy* **2020**, *45*, 34837–34844. [CrossRef]
21. Kramm, U.I.; Herrmann-Geppert, I.; Behrends, J.; Lips, K.; Fiechter, S.; Bogdanoff, P. On an easy way to prepare metal–nitrogen doped carbon with exclusive presence of MeN4-type sites active for the ORR. *J. Am. Chem. Soc.* **2016**, *138*, 635–640. [CrossRef] [PubMed]
22. Xue, Z.; Zhang, X.; Qin, J.; Liu, R. TMN4 complex embedded graphene as bifunctional electrocatalysts for high efficiency OER/ORR. *J. Energ. Chem.* **2021**, *55*, 437–443. [CrossRef]
23. Frisch, M.; Trucks, G.; Schlegel, H.; Scuseria, G.; Robb, M.; Cheeseman, J.; Scalmani, G.; Barone, V.; Mennucci, B.; Petersson, G.A.; et al. *Gaussian 09, Revision D. 01*; Gaussian, Inc.: Wallingford, CT, USA, 2009.
24. Ghildina, A.R.; Zavershinskiy, I.P.; Mebel, A.M.; Vinogradov, K.Y.; Bulanova, A.V.; Zhu, H. Theoretical Study of the Mechanism and Kinetics of the Oxidation of Cyclopenta[a]Naphthalenyl Radical C13H9 with Molecular Oxygen. *J. Phys. Chem. A* **2021**, *125*, 6796–6804. [CrossRef]
25. Lee, C.; Yang, W.; Parr, R.G. Development of the Colle-Salvetti correlation-energy formula into a functional of the electron density. *Phys. Rev. B* **1988**, *37*, 785. [CrossRef]

26. Vinogradov, K.Y.; Bulanova, A.V.; Shafigulin, R.V.; Tokranova, E.O.; Mebel, A.M.; Zhu, H. Density Functional Theory Study of the Oxygen Reduction Reaction Mechanism on Graphene Doped with Nitrogen and a Transition Metal. *ACS Omega* **2022**, *7*, 7066–7073. [CrossRef]

27. Quílez-Bermejo, J.; Melle-Franco, M.; San-Fabián, E.; Morallón, E.; Cazorla-Amorós, D. Towards understanding the active sites for the ORR in N-doped carbon materials through fine-tuning of nitrogen functionalities: An experimental and computational approach. *J. Mater. Chem. A* **2019**, *7*, 24239–24250. [CrossRef]

28. Yu, L.; Pan, X.; Cao, X.; Hu, P.; Bao, X. Oxygen reduction reaction mechanism on nitrogen-doped graphene: A density functional theory study. *J. Cat.* **2011**, *282*, 183–190. [CrossRef]

29. Liu, J.; Xiao, J.; Luo, B.; Tian, E.; Waterhouse, G.I.N. Central metal and ligand effects on oxygen electrocatalysis over 3d transition metal single-atom catalysts: A theoretical investigation. *Chem. Eng. J.* **2022**, *427*, 132038. [CrossRef]

30. Yang, Y.; Qi, W.; Niu, J.; Chen, F.; Li, W. Understanding active sites and mechanism of oxygen reduction reaction on FeN4–doped graphene from DFT study. *Int. J. Hydrogen Energy* **2020**, *45*, 15465–15475. [CrossRef]

31. Wei, P.; Li, X.; He, Z.; Sun, X.; Liang, Q.; Wang, Z.; Fang, C.; Li, Q.; Yang, H.; Han, J.; et al. Porous N, B co-doped carbon nanotubes as efficient metal-free electrocatalysts for ORR and Zn-air batteries. *Chem. Eng. J.* **2021**, *422*, 130134. [CrossRef]

32. Vashchenko, A.V.; Kuzmin, A.V.; Shainyan, B.A. Si-Doped Single-Walled Carbon Nanotubes as Potential Catalysts for Oxygen Reduction Reactions. *Russ. J. Gen. Chem.* **2020**, *90*, 454–459. [CrossRef]